

Reachability-based Adaptive UAV Scheduling and Planning in Cluttered and Dynamic Environments

Esen Yel and Nicola Bezzo

Abstract—Modern unmanned aerial vehicles (UAVs) rely on periodic sensor measurements and replanning operations to navigate through cluttered and dynamic environments. However, periodic sensor checking and replanning are time and energy consuming and can be relaxed if the UAV can make accurate assessments about its current and future states and safely navigate without colliding with any object. In this paper, we propose an adaptive framework that leverages reachability analysis and self- and event-triggered control schemes to schedule the next time to monitor sensors and trigger collision avoidance while guaranteeing safety under noise and disturbance effects. Replanning operations are further relaxed by proposing a risk-based approach that considers the deviation of the UAV from the planned trajectory. Finally, we validate the proposed approach with simulations in a cluttered environment with both static and dynamic obstacles case studies.

I. INTRODUCTION

In recent years, unmanned aerial vehicles (UAVs) have become more agile, autonomous and robust thanks to technological advancements in materials, computation power, sensing and actuation capabilities. These improvements have in order increased the interest in using such platforms in various applications such as search and rescue, reconnaissance and surveillance, delivery services, inspection, hobby and photography.

In most of these applications, generally, the UAV is required to travel to one or multiple goals following trajectories while sharing the airspace with other objects (either static or dynamic). In traditional approaches, the UAV checks its sensors periodically to detect the obstacles and replans its motion accordingly. However, periodic sensor checking and motion replanning are computationally expensive and they are not always necessary. This periodicity constraint can be relaxed if the system can assess and predict future states of itself and the obstacles under different uncertainties, which would minimize unnecessary energy and computation consumption resulting from sensor checking and motion replanning operations. For example, let us consider the pictorial representation in Fig. 1: a UAV flying in an obstacle free environment needs less computation time and can move faster than the same UAV navigating in a cluttered environment, in which it will need more computation time to elaborate sensor data and plan its trajectory to navigate through the environment without colliding with any obstacles. The same applied when dealing with collision avoidance with dynamic obstacles: if a collision is possible, the UAV will need to check and replan more often.

To deal with these problems, we propose an online reachability-based self-triggered scheduling and replanning

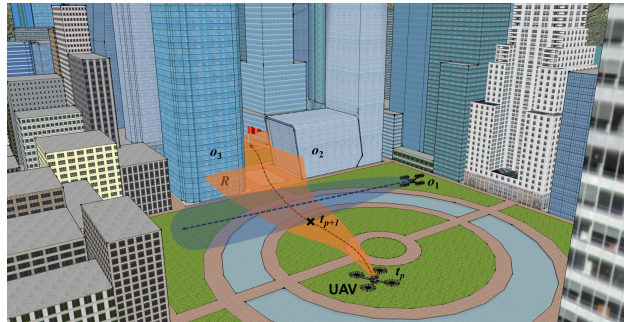


Fig. 1. Pictorial representation of the proposed problem in which a quadrotor UAV must navigate through a cluttered environment avoiding collision with both static and dynamic obstacles $\{o_1, o_2, o_3\}$ while minimizing periodic sensor checking under uncertainties like wind disturbances, noise, and jitter. R represents the reachable region of the UAV with t_{p+1} the first predicted time that a collision with o_1 may occur.

framework. In this work, we build upon our previous work [1], [2] in which we developed techniques for self-triggered replanning in cluttered and static environments. Specifically in this paper we further improve our technique by including a technique to delay replanning based on the reachability analysis and include dynamic obstacles (e.g., other vehicles) while guaranteeing safety. The proposed framework is based on the following consideration: *periodic checking, sensor monitoring and replanning are not always necessary, and can be relaxed if it is possible to predict and plan the operation of the robot considering uncertainties and the surrounding objects*. With these considerations in mind, this paper targets the development of a framework to solve the following challenges:

- how to minimize sensor checking and replanning operations, while guaranteeing safety properties;
- how to plan and replan a UAV operation to avoid collision while solving the previous challenge.

To this end, we utilize reachability analysis, self-triggered scheduling, and replanning policies to i) predict the future states of the system, ii) schedule the time for next sensor monitoring and motion replanning operation, iii) replan the motion of the UAV to avoid collisions under the effect of noise and unforeseen disturbance phenomena. The specific case studies presented in this work, and in particular in the simulation results, consider a UAV following a trajectory to reach a goal location in the environment while avoiding static and mobile obstacles. The aim of the robot is to adapt its motion, minimize its sensor monitoring and replanning operations, and avoid any collisions with objects in the environment.

II. RELATED WORK

In the last decade, we have witnessed to a rapid increase in research about unmanned aerial vehicles and in particular

Esen Yel and Nicola Bezzo are with the Departments of Systems and Information Engineering and Electrical and Computer Engineering, University of Virginia, Charlottesville, VA 22904, USA {esenyel, nbezzo}@virginia.edu

quadrotors. Motion planning along with obstacle and collision avoidance is one of the most significant capabilities which attracts researchers' attention in order to guarantee safety and robustness in autonomous operations. In the literature, we find numerous works dealing with collision avoidance, in case of both static and dynamic obstacles using different perception techniques. In [3], [4], an RGB-D sensor is used to detect the obstacles and estimate their positions. In [5], authors use an on-board limited field of view sensor to detect the mobile obstacles in the environment, and avoid them assuming that they have information about the obstacle dynamics. In [6], authors utilize Safe Flight Corridor concept to avoid the static obstacles detected with a 3D LiDAR sensor. In [7], an RRT based pre-planned path is modified according to the changes in the obstacle positions. In [8], moving obstacles are avoided using a reinforcement learning technique. In all of these works, obstacle detection is achieved via high-frequency periodic sensor data acquisition and elaboration.

In this work, we relax the sensor checking and replanning operations while guaranteeing safety in dynamic environments. We leverage reachability analysis to predict the future states of the system. Reachability analysis has been used for UAV operations for different purposes. In [9], the motion control inputs of an autonomous helicopter in an environment with disturbance are replanned according to the reach-avoid sets. In [10], dynamic obstacles are avoided using forward stochastic reachable sets. In [11], an aircraft is tasked to avoid other aircrafts by detecting collisions using reachable sets and sampling based methods are used to generate new trajectories to avoid obstacles. In [12], authors utilize reachable sets to detect collisions with other UAVs and to generate control laws for collision avoidance. In [13], a collision free trajectory is created by using Robust Control Invariant (RCI) tubes, which are defined as a region that the system state is guaranteed to stay within, under the presence of noise and disturbance. Differently from these previous works, we use reachable sets to: i) detect possible obstacle collisions over a future time horizon and ii) schedule next sensor checking and replanning events considering disturbance and uncertainties in the environment. In this paper we build on our previous works [1], [2] and extend our reachability-based self-triggered scheduling and replanning approach for the environments with mobile obstacles.

The rest of the paper is organized as follows: in Section IV, we formally define the problem. In Section III we outline the mathematical notation and assumptions used throughout this paper and in Section V, we define the UAV motion, noise, and disturbance models. Reachability analysis for both UAV operations and for dynamic obstacles is discussed in Section VI. Our self/event triggered scheduling and replanning approach is presented in Section VII, along with the simulations which validate our approach. Finally, we draw conclusions and discuss future work in Section VIII.

III. PRELIMINARIES

Through this paper we will denote vectors with bold lower case italic letters (e.g., \mathbf{x}) while matrices will be expressed with bold upper case italic letters (e.g., \mathbf{A}). $\|\cdot\|$ represents the Euclidean norm. The state of the UAV is denoted by

$\mathbf{q} \in \mathbb{R}^{12}$ and we use $\mathbf{p}_q \in \mathbb{R}^3$ to refer to the position part of the state. $\mathbf{x} \in \mathbb{R}^4$ is used to refer to the position and velocity part of the state in x-y direction and $\mathbf{p} \in \mathbb{R}^2$ denotes only the position in x-y direction.

In this work, we assume that the UAV is always able to observe its roll, pitch and yaw angles and angular velocities, as well as its z position and velocity. It is also assumed that the UAV can observe its position and velocity in $x-y$ plane (i.e. \mathbf{x}) via its sensor at scheduled times. The position of an obstacle in the $x-y$ plane is denoted by $\mathbf{o} \in \mathbb{R}^2$ with a subscript indicating the index of the obstacle and it is assumed to be observed via an on-board range sensor at scheduled times.

IV. PROBLEM FORMULATION

In this work we are interested in finding an online policy to schedule next sensor monitoring and replanning operations for a UAV navigating in a cluttered environment with both static and mobile obstacles. Formally, the problem can be casted as follows:

Problem 1: Self-triggered Replanning for Safe UAV Navigation in Cluttered and Dynamic Environments: A UAV has the objective to visit one or more goal locations in a cluttered and dynamic environment. The obstacle positions are detected using on-board range sensors and a trajectory with the desired goals is generated online according to the position of the detected obstacles. The goal is to find a scheduling policy to determine the next sensor monitoring and replanning time t_{p+1} , such that the UAV avoids collisions with obstacles between two consecutive replanning times, or mathematically:

$$\|\mathbf{p}(t) - \mathbf{o}_i(t)\| > 0, \forall t \in [t_p, t_{p+1}], \forall i \in [0, n_o] \quad (1)$$

in which $\mathbf{p}(t) = [x, y]^T$ is the position of the UAV and $\mathbf{o}_i(t) = [o_x(t), o_y(t)]^T$ is the position of the i^{th} obstacle in the $x-y$ plane at time t with n_o the number of obstacles in the environment.

V. SYSTEM MODELS

In this section, we present the dynamics, noise, and disturbance models that will be used to control the UAV and compute reachable sets. Here, we follow the architecture shown in Fig. 2 and describe its main elements as follows.

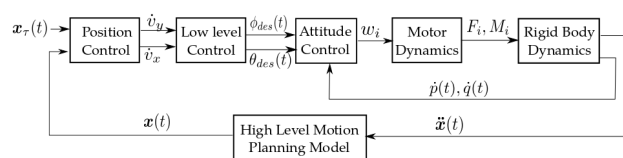


Fig. 2. UAV planning and control architecture.

A. Quadrotor Dynamical Model

A quadrotor can be modeled using the following 12th order state vector:

$$\mathbf{q} = [\mathbf{p}_q^T \quad \phi \quad \theta \quad \psi \quad v_x \quad v_y \quad v_z \quad \omega_x \quad \omega_y \quad \omega_z]^T$$

where $\mathbf{p}_q = [x \ y \ z]^T$ is the world frame position, v_x, v_y and v_z are the world frame velocities, ϕ, θ and ψ are the roll, pitch and yaw Euler angles and ω_x, ω_y and ω_z are the body frame angular velocities [1], [14].

The dynamics of the quadrotor can be described as:

$$\begin{aligned} \dot{\mathbf{p}}_q^\top &= [v_x \ v_y \ v_z] \\ \begin{bmatrix} \dot{v}_x \\ \dot{v}_y \\ \dot{v}_z \end{bmatrix} &= \begin{bmatrix} 0 \\ 0 \\ -g \end{bmatrix} + \frac{1}{m} \begin{bmatrix} \cos \phi \cos \psi \sin \theta + \sin \phi \sin \psi \\ \cos \phi \sin \theta \sin \psi - \cos \psi \sin \phi \\ \cos \theta \cos \phi \end{bmatrix} u_1 \\ \begin{bmatrix} \dot{\phi} \\ \dot{\theta} \\ \dot{\psi} \end{bmatrix} &= \begin{bmatrix} 1 & \sin \phi \tan \theta & \cos \phi \tan \theta \\ 0 & \cos \phi & -\sin \phi \\ 0 & \sin \phi \sec \theta & \cos \phi \sec \theta \end{bmatrix} \begin{bmatrix} \omega_x \\ \omega_y \\ \omega_z \end{bmatrix} \\ \begin{bmatrix} \dot{\omega}_x \\ \dot{\omega}_y \\ \dot{\omega}_z \end{bmatrix} &= \begin{bmatrix} \frac{I_{yy} - I_{zz}}{I_{xx}} \omega_y \omega_z \\ \frac{I_{zz} - I_{xx}}{I_{yy}} \omega_x \omega_z \\ \frac{I_{xx} - I_{yy}}{I_{zz}} \omega_x \omega_y \end{bmatrix} + \begin{bmatrix} \frac{1}{I_{xx}} & 0 & 0 \\ 0 & \frac{1}{I_{yy}} & 0 \\ 0 & 0 & \frac{1}{I_{zz}} \end{bmatrix} \begin{bmatrix} u_2 \\ u_3 \\ u_4 \end{bmatrix} \end{aligned}$$

B. High-Level Motion Planning Model

The following high-level motion planning model is used to capture the quadrotor position and velocity evolutions in the $x - y$ plane. This simplified model will be used for the reachability analysis presented in the next section.

$$\begin{aligned} \dot{\mathbf{x}}(t) &= \mathbf{A}\mathbf{x}(t) + \mathbf{B}(\mathbf{u}(t) + \eta_u) + \mathbf{G}\mathbf{d}(t) \\ \mathbf{y}(t) &= \mathbf{C}\mathbf{x}(t) + \eta_x \end{aligned} \quad (2)$$

where $\mathbf{x} = [x \ y \ v_x \ v_y]^\top$ is the state, \mathbf{y} is the sensor measurement vector with sensor noise vector η_x . \mathbf{u} is the input acceleration with input noise η_u , and $\mathbf{d} = [d_x \ d_y]^\top$ is the disturbance. \mathbf{A} , \mathbf{B} , \mathbf{G} and \mathbf{C} matrices are given by:

$$\mathbf{A} = \begin{bmatrix} 0 & 0 & 1 & 0 \\ 0 & 0 & 0 & 1 \\ 0 & 0 & 0 & 0 \\ 0 & 0 & 0 & 0 \end{bmatrix} \quad \mathbf{B} = \begin{bmatrix} 1 & 0 \\ 0 & 1 \\ 1 & 0 \\ 0 & 1 \end{bmatrix} \quad \mathbf{G} = \begin{bmatrix} 1 & 0 \\ 0 & 1 \\ k_x & 0 \\ 0 & k_y \end{bmatrix} \quad \mathbf{C} = \mathbf{I}$$

where k_x and k_y are the drag parameters in x and y direction respectively and \mathbf{I} is a 4×4 identity matrix.

This model assumes that the quadrotor is moving at a constant z level with a zero yaw constraint. The block diagram in Fig. 2 shows the relationship between the complete quadrotor dynamics and the high level motion planner model.

C. Position, Low Level, and Attitude Controls

Following the architecture in Fig. 2, the position and low-level controllers (implemented as a series of PID loops after linearizing (V-A), [15]) generate the necessary angle inputs to the attitude control in order to follow the desired trajectory \mathbf{x}_τ . The attitude controller along with the motor dynamics calculate the thrust and moment values that each rotor should provide for these angle inputs [14], [15]. Finally the rigid body dynamics generate the response of the quadrotor to these thrust and moment values in terms of acceleration. The position and low level controller errors are represented as input noise in the high level motion planning model (2). This is described in more detail in the following section.

D. Noise and Disturbance Model

When a quadrotor is flying, internal factors like sensor or actuator noises or external factors like wind disturbance may cause it to deviate from its planned behavior and they all should be taken into consideration for safety. In this work, we assume that environmental disturbance, actuator noise, and state uncertainty are all bounded by ellipsoids

and uniformly distributed. It should be noted that beside simplifying the calculation of reachable sets, this is a valid assumption because uncertainties with very low probability can be neglected and thus can be bounded. The uniform distribution assumption is also valid in this case since the considered truncated uncertainties are treated in the same way from a safety point of view. The state uncertainty caused by the sensor measurement noise is represented by $\eta_x \in \epsilon(0, N_x)$ which represents an ellipsoid centered in the origin and bounded by a shape matrix N_x . The sources of the input uncertainties η_u are the actuator and process noises resulting from the low-level controllers and the mechanical uncertainties from the rotors, gears, and propellers. The input uncertainty is assumed to be bounded by an ellipsoid, $\eta_u \in \epsilon(0, N_u)$ where N_u is the bound. The external disturbance $\mathbf{d}(t)$ is also centered around the origin and bounded by an ellipsoid $\mathbf{d}(t) \in \epsilon(0, N_d)$ where N_d is the disturbance bound.

VI. REACHABILITY ANALYSIS

In order to predict the future states of the system and the obstacle, and utilize that information to decide next sensor monitoring and replanning time, we leverage reachability analysis (RA).

A. Reachability Analysis for UAV Operations

A *reachable set* or *reach set* of a system is defined as the set of states such that for each of them there exists an input which drives the system from its initial point to this state over a certain time window. In order to calculate reachable set of the UAV, we leverage the reachability analysis presented in [16]. A reachable set computed at time t_0 for a future time t_f and represented by $R(\mathbf{x}_0, \mathbf{u}(t), t_f)$ is an ellipsoid ϵ that contains all the states \mathbf{x} reachable at a future time $t_f > t_0$ where the initial set $\mathbf{x}_0 \in \epsilon(\mathbf{x}_0, \mathbf{X}_0)$ is bounded by an ellipsoid with center \mathbf{x}_0 and shape matrix \mathbf{X}_0 and the input $\mathbf{u}(t) \in \epsilon(\mathbf{u}(t), \mathbf{U})$ is bounded by an ellipsoid with center $\mathbf{u}(t)$ and shape matrix \mathbf{U} . The actual state $\mathbf{x}(t_f)$ and the estimated state $\tilde{\mathbf{x}}(t_f)$ will lie inside the reachable ellipsoid. The shape matrix \mathbf{X}_0 of the initial state ellipsoid depends on the state uncertainty η_x whereas the shape matrix of the input ellipsoid \mathbf{U} depends on the input uncertainty η_u as explained in Section V-D. $R_p(\mathbf{x}_0, \mathbf{u}(t), t_f)$ is the projection of the reachable sets on the position space and a reachable tube $R(\mathbf{x}_0, \mathbf{u}(t), [0, T])$ is the set of all reachable sets over the time interval $\Delta T = [0, T]$.

The external bound for the reach set at time t starting from an initial time t_0 is calculated based on the initial state ellipsoid, the plant model, the input ellipsoid, and the disturbance ellipsoid as follows:

$$\begin{aligned} R^+(t, t_0, \epsilon(\mathbf{x}_0, \mathbf{X}_0)) &= (\Phi(t, t_0)\epsilon(\mathbf{x}_0, \mathbf{X}_0) \\ &\oplus \int_{t_0}^t \Phi(t, \zeta)\mathbf{B}\epsilon(\mathbf{u}(\zeta), \mathbf{U})d\zeta \\ &\ominus \int_{t_0}^t \Phi(t, \zeta)(-\mathbf{G})\epsilon(0, N_d)d\zeta \end{aligned}$$

where $\Phi(t, t_0) = e^{\mathbf{A}(t-t_0)}$ and the symbols \oplus and \ominus represent geometric sum and geometric difference respectively.

In this work, we calculate the reachable sets of the states of a quadrotor tracking a trajectory $\mathbf{x}_\tau(t_p : t_{p+1})$ generated over the interval $\Delta t_p = [t_p, t_{p+1}]$ where t_p is the current planning time and t_{p+1} is the next planning time, initially set to $t_p + T$ before the rescheduling operation. We generate minimum jerk trajectory [17], and an online simulator implementing a PD controller is used to find the acceleration inputs to track this trajectory as if there is no disturbance and noise in the environment. These computed inputs are used to calculate the reachable tubes. In Fig. 3, a position reachable tube calculated for $\Delta t_p = 2$ s is shown for a quadrotor moving in the x direction with sensor measurement noise $\eta_x = 0.001$ and input noise $\eta_u = 0.054$. Although the actual path of the quadrotor (blue dotted curve) is different from its desired trajectory (red star curve) due to wind disturbance $\mathbf{d} = [0.1, 0.1]$ m/s, it is contained inside the reachable tubes, since uncertainties and disturbances are taken into account in the reachable tube calculation.

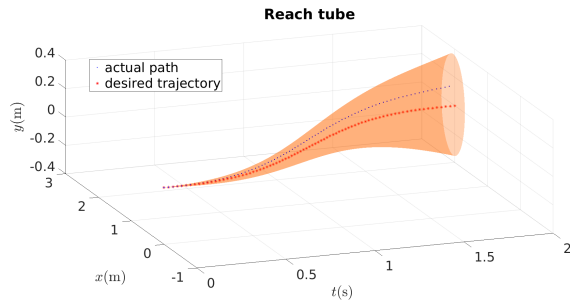


Fig. 3. The position reachable tube for a quadrotor following a straight line trajectory for 2s.

B. Dynamic Obstacle Reachability Analysis

In order to guarantee a safe operation of a UAV in a cluttered and dynamic environment without monitoring the sensors constantly, the future states of dynamic obstacles are required to be predicted. To capture the possible future states of a mobile obstacle, we calculate their reachable sets based on the available information about their state, maximum velocity and direction. For the sake of simplicity, we assume that the obstacle has a known maximum speed $v_{o,max}$, and a heading not known a priori. Therefore, at the initial planning time t_0 , the position reachable set of the obstacle, $R_p^o(\mathbf{o}_i(t_0), [t_0 + T])$, is a circle centered around the obstacle position as shown in Fig. 5(a), which contains all the points reachable within the planning horizon T . The direction and velocity of the obstacle at time t_p , $\vec{v}_{oi}(t_p)$, can be estimated based on previous observations about its position state, as follows:

$$\vec{v}_{o,i}(t_p) = \frac{\mathbf{o}_i(t_p) - \mathbf{o}_i(t_{p-1})}{\|\mathbf{o}_i(t_p) - \mathbf{o}_i(t_{p-1})\|}, \quad \forall i \in [0, n_o] \quad (3)$$

Its reachable set can be constructed along its trajectory taking into account estimation errors and noise as depicted in Fig. 5(b). Due to measurement noise and uncertainties, the actual direction of the obstacle might differ from the estimated one. However it can be bounded. The minimum and maximum limits of the direction of the UAV can be

calculated as follows:

$$\vec{v}_{o,i}^+(t_p) = \frac{\mathbf{o}_i^+(t_p) - \mathbf{o}_i(t_{p-1})}{\|\mathbf{o}_i^+(t_p) - \mathbf{o}_i(t_{p-1})\|}, \quad \forall i \in [0, n_o] \quad (4)$$

$$\vec{v}_{o,i}^-(t_p) = \frac{\mathbf{o}_i^-(t_p) - \mathbf{o}_i(t_{p-1})}{\|\mathbf{o}_i^-(t_p) - \mathbf{o}_i(t_{p-1})\|}, \quad \forall i \in [0, n_o] \quad (5)$$

where $\vec{v}_{o,i}^+(t_p)$ and $\vec{v}_{o,i}^-(t_p)$ are upper and lower limits of the direction of the obstacle where $\mathbf{o}_i^+(t_p)$ and $\mathbf{o}_i^-(t_p)$ are two extreme points where the obstacle can be at t_p as seen in Fig. 4 where η_x is the maximum measurement noise.

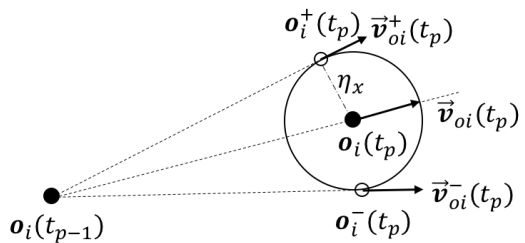


Fig. 4. Calculation of the obstacle direction based on the previous position of the obstacle and the magnitude of uncertainties.

The updated reach set of the obstacle based on its current position and the direction for time horizon T is shown in Fig. 5(b) with blue shaded region. As can be noticed, the reachable set of the obstacle grows in its nominal direction with the rate of its maximum velocity.

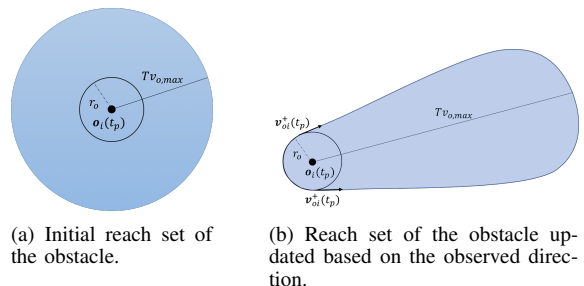


Fig. 5. Initial and updated reach sets of the obstacle.

VII. SELF/EVENT-TRIGGERED SCHEDULING AND REPLANNING

In this section, we describe our framework for self/event triggered scheduling and replanning for UAV operations in both cluttered and dynamic environments. In order to efficiently use the available computational resources, it is desirable to limit the sensor monitoring and replanning operations to the instances when it is really necessary while guaranteeing safety. In traditional motion planning approaches, sensor monitoring and replanning occur in a time-periodic fashion, without considering the state information. In this work, we present self-triggered scheduling and self/event-triggered replanning policies to decide next sensor monitoring and replanning times based on the information available about the UAV and the obstacles states at planning time. This idea is closely related to the work on self-triggered control presented in [18] in which the authors outline a technique

that enables a controller to decide its next execution time while maintaining stability. We extend this methodology to consider the replanning case and instead of stability issues here we consider safety cost constraints.

In the following section, we present our self-triggered scheduling and replanning approach for the operations in cluttered environments, which is based on our previous work [2].

A. Self-triggered Scheduling and Replanning in Cluttered Environments

In this work we propose a self-triggered scheduling and replanning framework to decide the next sensor monitoring and replanning time to minimize computation power. At the beginning of the operation, based on the observations about the static obstacles positions, a trajectory to go to the desired goal position \mathbf{x}_g and to avoid the obstacles is generated. Using the desired trajectory and control input values to follow this trajectory, reachable tubes of the UAV is generated as outlined in Section VI-A and self-triggered scheduling policy leverage them to determine next sensor monitoring and replanning time. To further minimize the number of replanning operations, a risk-based rescheduling approach is used to update the reachable tubes without recalculating the trajectory. The overall architecture of our self-triggered scheduling and replanning policy is summarized in Fig. 6.

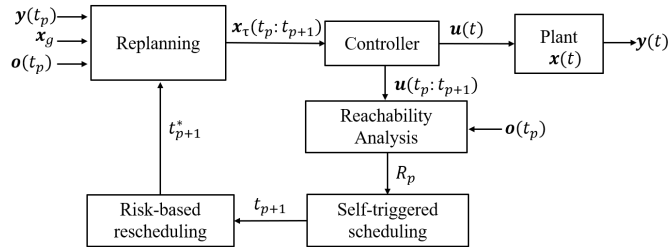


Fig. 6. Overall self-triggered scheduling and replanning framework in cluttered environments.

1) *Self-triggered Scheduling*: In order to decide the next replanning time t_{p+1} , the reachability analysis is leveraged to guarantee safety between replanning operations. The predicted first time that a collision may occur, t_c , is calculated using the position reachable tube presented in Section VI-A as follows:

$$t_c = \min(t_k | R_p(\mathbf{x}_0, \mathbf{u}(t_k), t_k \in [t_p, t_p + T]) \cap \mathcal{O} \neq \emptyset) \quad (6)$$

where $\mathcal{O} \in \mathbb{R}^{2 \times n_o}$ is the set of obstacle positions and n_o is the number of obstacles in the environment.

The earliest time that the UAV can leave the region covered by the field of view of its range sensor, denoted by t_l is calculated as follows:

$$t_l = \min(t_k | R_p(\mathbf{x}_0, \mathbf{u}(t_k), t_k \in [t_p, t_p + T]) \not\subset \mathbf{r}(t_p)) \quad (7)$$

where $\mathbf{r}(t_p)$ is the set of all points in the $x-y$ plane covered by the range sensor of the UAV at the planning time t_p .

If there is a possibility to collide with an obstacle or leave the region covered by the range sensor, the UAV needs to check its state to decide whether replanning is necessary or not. Therefore, it needs to check its state either at time t_c ,

or at the time t_l , whichever is the minimum. If it is not possible to collide with any obstacle or leave the sensor field of view within the planned horizon T , then monitoring and replanning happen at time T .

$$t_{p+1} = \begin{cases} \min(t_c, t_l) - t_r, & \text{if } t_c < T \text{ or } t_l < T \\ T - t_r, & \text{otherwise} \end{cases} \quad (8)$$

where t_r is the amount of time necessary for the replanning calculation. Using this approach, we can guarantee to stay within the sensor field of view and avoid collisions with any obstacles. A formal safety proof of our self-triggered scheduling approach is presented in [2].

2) *Risk-based Rescheduling*: Reachable tubes are meant to capture the worst case scenario in terms of disturbance and noise, therefore they tend to grow very large over time. Therefore, replanning at each time that the reachable tube collides with an obstacle may be over-conservative and recalculating the reachable tubes would bring more computational burden. To overcome this limitation and postpone next monitoring and replanning operations we leverage the deviation from the desired trajectory at each scheduling time to update the current reachable sets without the need to recalculate it. The deviation from the desired trajectory at replanning time can be calculated as follows:

$$d(t_{p+1}) = \|\mathbf{p}(t_{p+1}) - \mathbf{p}_\tau(t_{p+1})\|$$

where $\mathbf{p}(t_{p+1})$ is the position of the UAV at time t_{p+1} and $\mathbf{p}_\tau(t_{p+1})$ is the desired position on the planned trajectory at t_{p+1} . The external bound of the position reachable tube $R_p^+(t, t_p, \epsilon(\mathbf{x}(t_p), \mathbf{X}_{t_p}))$ can be shrunk by $r_t(t_{p+1}) - d(t_{p+1})$ where $r_t(t_{p+1})$ is the radius of the reachable tube at time t_{p+1} , since it becomes impossible for the system to reach the previously computed reachable tube border. Fig. 7 is a pictorial representation of reachable tube update procedure. In Fig. 7, the original reachable tube is shown by shaded orange area. At time t_{p+1} , based on the deviation from the desired trajectory and the radius of the original reachable tube, the original reachable tube shrunk to a smaller one shown with the darker orange region. Utilizing the self-triggered scheduling with the updated smaller reachable tubes, next replanning time t_{p+1}^* can then be calculated using the same approach outlined in Section VII-A.1. Hence, by using this approach, next replanning time can be postponed to a future time, saving more computation overhead.

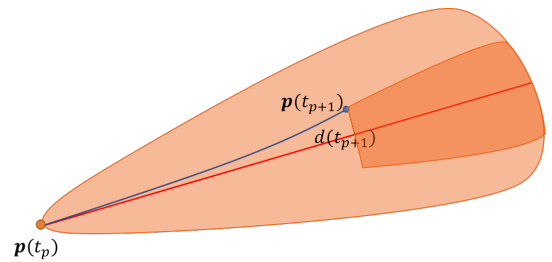


Fig. 7. Updating the reachable tubes based on the deviation from the desired trajectory.

3) *Simulations with Static Obstacles*: Here we present simulation results for a UAV waypoint navigation in a cluttered environment while performing the proposed online self-triggered scheduling and replanning approach. We consider a quadrotor UAV equipped with a localization sensor (e.g. GPS) and a range sensor (e.g. a lidar) with a limited 10m range and a 180° field of view. Starting from the origin, the UAV is tasked to go to a goal position 30m away. A constant wind disturbance of magnitude $\mathbf{d} = [-0.07, 0.07]^T$ m/s is present everywhere in the environment and unknown a priori. The UAV plans its trajectory to avoid the obstacles along its way and use the described self-triggered scheduling approach to determine next sensor checking time and replanning times. It also calculates a risk to postpone replanning time at the points shown by magenta '◇' symbols. Using this approach, the UAV performs only 8 replanning operations at points shown by black '×' symbols and follows its trajectory with a maximum deviation of 5.80cm and an average deviation of 4.16cm.

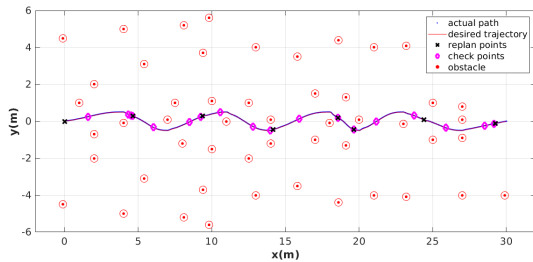


Fig. 8. Simulation results for a UAV waypoint navigation in cluttered and static environments running the proposed risk-based self-triggered scheduling and replanning approach. The desired trajectory (red curve) is compared with the actual path (blue dots) of the quadrotor with our approach. The UAV calculates the risk at points shown by magenta '◇' symbols and replan its motion at points shown by black '×' symbols.

B. Self/Event-Triggered Scheduling and Replanning in Dynamic Environments

In this section we describe a self/event-triggered scheduling and replanning framework for dynamic obstacles. We follow the architecture in Fig. 9.

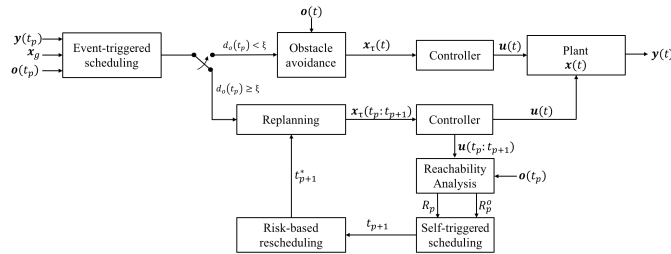


Fig. 9. Overall self/event-triggered scheduling and replanning framework in dynamic environments.

Based on the initial observations about the obstacle positions, a trajectory to the desired goal position \mathbf{x}_g is generated. Next sensor monitoring time is determined leveraging reachability analysis to predict the future states of the UAV as outlined in Section VI-A and to predict the future states of the obstacles as presented in Section VI-B. If this distance

$d_o(t_p)$ between the UAV and the closest mobile obstacle is smaller than a user defined threshold ξ , an obstacle avoidance behavior is triggered in which sensor checking switches to be periodic. Collision avoidance is then performed using repulsive potential fields, [19].

1) *Self/Event-triggered Scheduling and Replanning*: In a dynamic environment, the first time a collision may occur, $t_{c,o}$, is calculated as follows:

$$t_{c,o} = \min(t_k | R_p(\mathbf{x}_0, \mathbf{u}(t_k), t_k \in [t_p, t_p + T]) \cap R_p^o(\mathbf{o}_i(t_p), t_k \in [t_p, t_p + T]) \neq \emptyset)$$

where $R_p^o(\mathbf{o}_i(t_p), t_k \in [t_p, t_p + T])$ is the geometric sum of the position reachable sets of the obstacle between t_p and $t_p + T$. Fig. 10 shows a simulation result in which the reachable set of the obstacle collides with the reachable tube of the UAV for the first time at $t_{c,o}$.

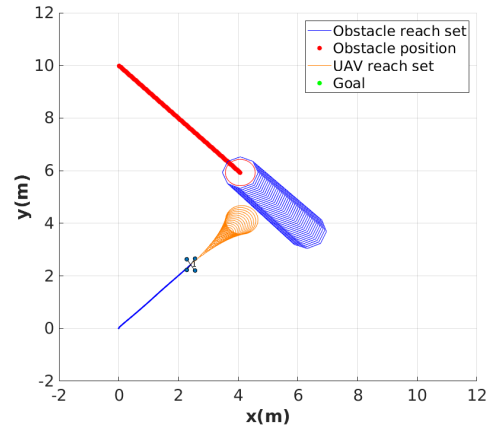


Fig. 10. Collision between the reachable tube of the UAV and reachable set of the obstacle at time $t_{c,o}$.

Similar to the case with static obstacles, the next sensor checking time is scheduled to t_l or $t_{c,o}$ whichever is minimum:

$$t_{p+1} = \begin{cases} \min(t_{c,o}, t_l) - t_r, & \text{if } t_{c,o} < T \text{ or } t_l < T \\ T - t_r, & \text{otherwise} \end{cases} \quad (9)$$

/a where t_r is the amount of time necessary for the replanning calculation.

2) *Dynamic Obstacle Repulsive Potential Field Collision Avoidance*: If $d_o(t_p) < \xi$ a collision avoidance is initiated following a repulsive potential field approach. The repulsive potential field around the reachable set of the obstacle $W_O(\mathbf{p}(t))$ can be computed as follows:

$$W_O(\mathbf{p}(t)) = \begin{cases} \frac{1}{2} \alpha_i \left(\frac{1}{\rho(\mathbf{p}(t))} - \frac{1}{\rho_0} \right)^2, & \text{if } \rho(\mathbf{p}(t)) \leq \rho_0 \\ 0, & \text{if } \rho(\mathbf{p}(t)) > \rho_0 \end{cases} \quad (10)$$

where $\rho(\mathbf{p}(t))$ is the shortest distance to the obstacle reachable tube from the position of UAV $\mathbf{p}(t)$, ρ_0 is distance threshold for the repulsive field and α_i is a positive constant. Then the repulsive force $F_O(\mathbf{p}(t))$ is equal to negative gradient of $W_O(\mathbf{p}(t))$:

$$F_O(\mathbf{p}(t)) = \alpha_i \left(\frac{1}{\rho(\mathbf{p}(t))} - \frac{1}{\rho_0} \right) \frac{1}{\rho(\mathbf{p}(t))^2} \nabla \rho(\mathbf{p}(t)) \quad (11)$$

The attractive potential field $W_G(\mathbf{p}(t))$ to go to the goal position is calculated as follows:

$$W_G(\mathbf{p}(t)) = \frac{1}{2}\zeta_i(\|\mathbf{p}(t) - \mathbf{x}_g\|^2) \quad (12)$$

where \mathbf{x}_g is the position of the goal and ζ_i is a positive constant. The attractive force is the gradient of the attractive field at $\mathbf{p}(t)$:

$$F_G(\mathbf{p}(t)) = -\zeta_i(\mathbf{p}(t) - \mathbf{x}_g) \quad (13)$$

Finally, the UAV moves with the combination of repulsive and attractive forces:

$$F(\mathbf{p}(t)) = F_G(\mathbf{p}(t)) + F_O(\mathbf{p}(t)) \quad (14)$$

As soon as $d_o(t_p) \geq \xi$ the UAV switches back to the self/event-triggered scheduling policy presented above.

3) *Simulations with a Dynamic Obstacle*: In this section, a UAV waypoint navigation through a simple environment with one mobile obstacle intersecting its path while under sensor and process noises and wind disturbance. We consider the same UAV described in Section VII-A. A constant wind disturbance of magnitude $\mathbf{d} = [-0.07, 0.07]^T$ m/s is present everywhere in the environment and unknown a priori.

In the simulations shown in Fig. 11, the UAV is tasked to go to a goal point $\mathbf{x}_g = [10, 10]$ m shown by a green circle. A dynamic obstacle, shown by a red circle, moves towards the path of the UAV however since the obstacle is faster than the UAV in this case, their trajectories do not collide with each other. The first three figures in Fig. 11 display the positions of the obstacle and UAV before, near and after the intersection point respectively. As can be seen, the UAV follows a straight path without performing any maneuvers to avoid the obstacle since the obstacle passes the intersection point earlier than the UAV. The replanning occurs only 2 times at the points shown by black ‘x’ symbols in Fig. 11(d). At the points shown by magenta ‘diamond’ symbols, the UAV checks its sensors but doesn’t replan its trajectory. In this simulation, the average and maximum deviation from the desired trajectory is recorded as 6.44cm and 9.25cm respectively.

In Fig. 12, the UAV is tasked to go to a goal point $\mathbf{x}_g = [6, 10]$ m. A dynamic obstacle moves towards its trajectory and in this case they could collide with each other at the intersection point of their trajectories if the trajectory is not replanned. The first figure in Fig. 12 shows the path of the obstacle and the UAV before the intersection point. As they get closer to each other, our event-triggered replanning approach triggers the obstacle avoidance behavior and the UAV starts to deviate from its planned trajectory to avoid collision with the obstacle. After the UAV passes the obstacle, as shown in Fig. 12(c), and it’s far from the obstacle, it goes back to its original self-triggered planning toward the goal. In this case, the UAV replans its trajectory only 3 times at the points shown by black ‘x’ symbols in Fig. 12(d). At the points shown by magenta ‘diamond’ symbols, the UAV checks its sensors but doesn’t replan its trajectory, and as can be seen, while avoiding the obstacle, it constantly checks its sensor. In this simulation, the average and maximum deviation from the desired trajectory is recorded as 4.71cm and 7.77cm respectively.

In Fig. 13, the UAV is tasked to go to a goal point $\mathbf{x}_g = [10, 10]$ m. A dynamic obstacle approaches the UAV from the opposite direction. The first figure in Fig. 13 shows the paths of the obstacle and the UAV before reaching the intersection point. Similar to the previous case, as they get closer to each other, our event-triggered replanning approach triggers a collision avoidance behavior. After the UAV passes the obstacle, as shown in Fig. 12(c), it goes back to the original self-triggered behavior towards its goal. In this case, the UAV replans its trajectory only 4 times at the black ‘x’ marks in Fig. 13(d). In this simulation, the average and maximum deviation from the desired trajectory is recorded as 6.01cm and 11.45cm respectively.

VIII. CONCLUSION AND FUTURE WORK

In this work, we have presented a self/event-triggered policy for UAV motion planning in cluttered and dynamic environments under the effect of uncertainties and disturbances. Our approach considers: 1) reachability analysis to predict the future states of the system and predict collisions with static and dynamic obstacles, 2) a self-triggered policy to schedule the next replanning operation, 3) an event-triggered policy to trigger collision avoidance all while minimizing sensor and replanning operations. To further minimize the replanning operations, a risk-based approach is proposed that shrink previously computed reachable sets based on the deviation of the UAV. Using the proposed techniques, we demonstrated that the sensor monitoring and replanning operations can be relaxed to minimize computation, and thus energy consumption.

In the future we also plan to use a similar framework to optimize energy consumption leaving sensors in idle mode when not in use. Further, we plan to incorporate machine learning techniques to consider cases in which the model of the vehicle is unknown or changes due to failures.

ACKNOWLEDGMENTS

This work is based on research sponsored by ONR under agreement number N000141712012.

REFERENCES

- [1] E. Yel, T. X. Lin, and N. Bezzo, “Reachability-based self-triggered scheduling and replanning of uav operations,” in *NASA/ESA Conference on Adaptive Hardware and Systems*, July 2017, pp. 221–228.
- [2] —, “Self-triggered adaptive planning and scheduling of uav operations,” in *IEEE International Conference on Robotics and Automation (ICRA)(to appear)*, May 2018.
- [3] M. C. P. Santos, L. V. Santana, A. S. Brando, and M. Sarcinelli-Filho, “Uav obstacle avoidance using rgb-d system,” in *International Conference on Unmanned Aircraft Systems*, June 2015, pp. 312–319.
- [4] M. C. P. Santos, C. D. Rosales, M. Sarcinelli-Filho, and R. Carelli, “A novel null-space-based uav trajectory tracking controller with collision avoidance,” *IEEE/ASME Transactions on Mechatronics*, vol. 22, no. 6, pp. 2543–2553, Dec 2017.
- [5] S. Roelofsen, D. Gillet, and A. Martinoli, “Reciprocal collision avoidance for quadrotors using on-board visual detection,” in *IEEE/RSJ International Conference on Intelligent Robots and Systems (IROS)*, Sept 2015, pp. 4810–4817.
- [6] S. Liu, M. Watterson, K. Mohta, K. Sun, S. Bhattacharya, C. J. Taylor, and V. Kumar, “Planning dynamically feasible trajectories for quadrotors using safe flight corridors in 3-d complex environments,” *IEEE Robotics and Automation Letters*, vol. 2, no. 3, pp. 1688–1695, July 2017.
- [7] M. Otte and E. Frazzoli, “RRT X: Real-time motion planning/replanning for environments with unpredictable obstacles,” in *Algorithmic Foundations of Robotics XI*. Springer, 2015, pp. 461–478.

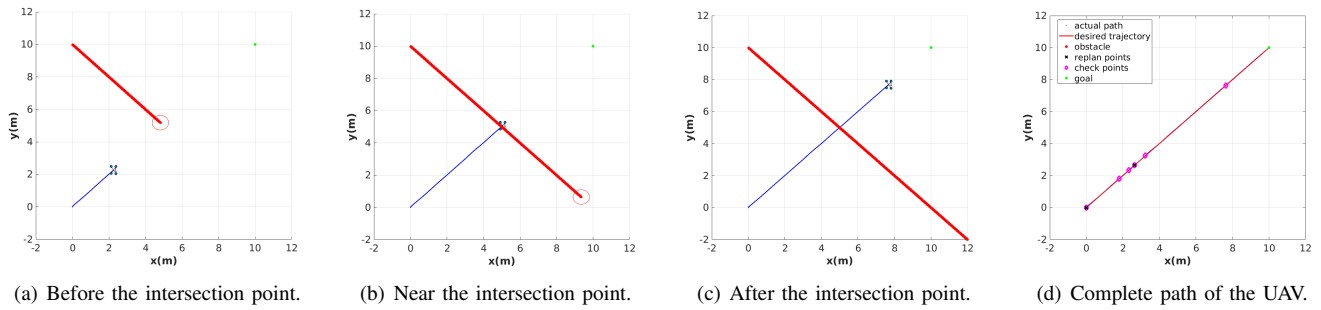


Fig. 11. Simulation Results in which the paths of the UAV and the obstacle intersects but collision doesn't happen because the obstacle passes the intersecting point earlier than the UAV.

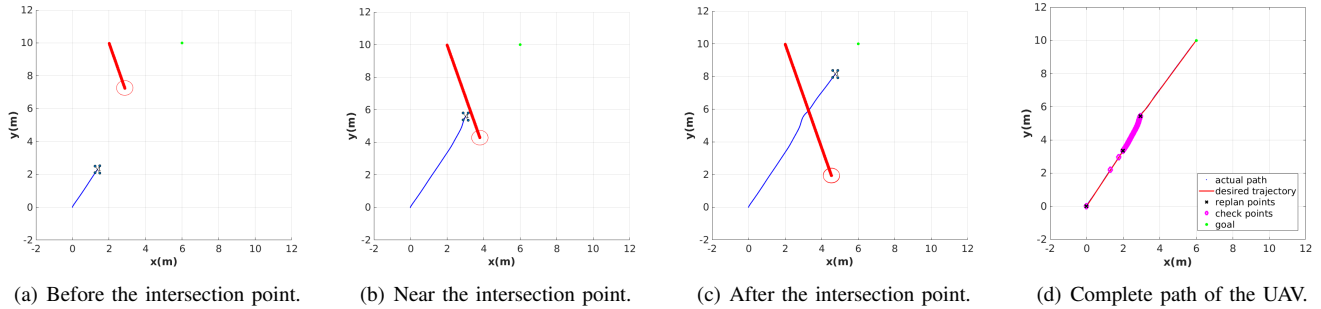


Fig. 12. Simulation results of collision avoidance. The obstacle and the UAV could collide with each other without replanning.

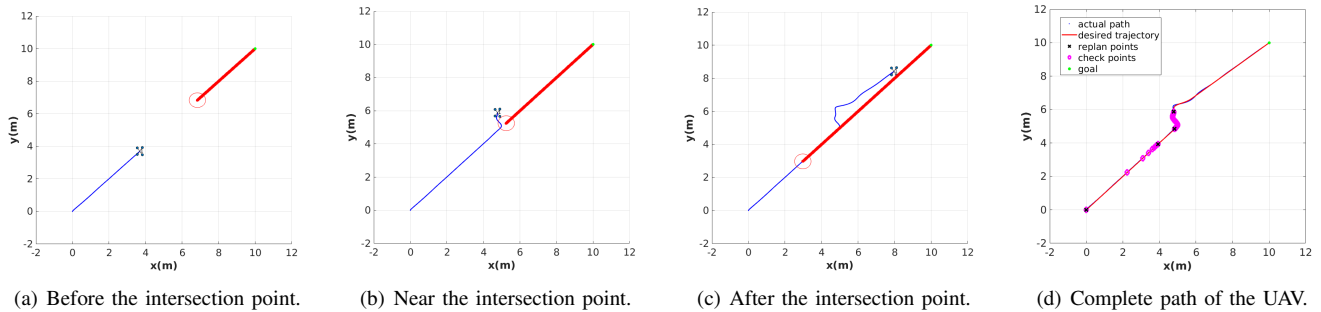


Fig. 13. Simulation results of collision avoidance in which the obstacle and the UAV move towards each others.

- [8] A. Faust, H. T. Chiang, N. Rackley, and L. Tapia, "Avoiding moving obstacles with stochastic hybrid dynamics using pearl: Preference appraisal reinforcement learning," in *IEEE International Conference on Robotics and Automation (ICRA)*, May 2016, pp. 484–490.
- [9] J. Ding, E. Li, H. Huang, and C. J. Tomlin, "Reachability-based synthesis of feedback policies for motion planning under bounded disturbances," in *IEEE International Conference on Robotics and Automation*, May 2011, pp. 2160–2165.
- [10] A. P. Vinod, B. Homchaudhuri, and M. M. K. Oishi, "Forward stochastic reachability analysis for uncontrolled linear systems using fourier transforms," *CoRR*, vol. abs/1610.04550, 2016. [Online]. Available: <http://arxiv.org/abs/1610.04550>
- [11] Y. Lin and S. Saripalli, "Sampling-based path planning for uav collision avoidance," *IEEE Transactions on Intelligent Transportation Systems*, vol. PP, no. 99, pp. 1–14, 2017.
- [12] Y. Zhou, A. Raghavan, and J. S. Baras, "Time varying control set design for uav collision avoidance using reachable tubes," in *IEEE 55th Conference on Decision and Control (CDC)*, Dec 2016, pp. 6857–6862.
- [13] S. Singh, A. Majumdar, J. J. Slotine, and M. Pavone, "Robust online motion planning via contraction theory and convex optimization," in *IEEE International Conference on Robotics and Automation (ICRA)*, May 2017, pp. 5883–5890.
- [14] N. Bezzo, K. Mohta, C. Nowzari, I. Lee, V. Kumar, and G. Pappas, "Online planning for energy-efficient and disturbance-aware uav operations," in *IEEE/RSJ International Conference on Intelligent Robots and Systems (IROS)*, Oct 2016, pp. 5027–5033.
- [15] N. Michael, D. Mellinger, Q. Lindsey, and V. Kumar, "The grasp multiple micro-uav testbed," *IEEE Robotics Automation Magazine*, vol. 17, no. 3, pp. 56–65, Sept 2010.
- [16] A. A. Kurzhanskiy and P. Varaiya, "Ellipsoidal toolbox (et)," in *Proceedings of the 45th IEEE Conference on Decision and Control*, Dec 2006, pp. 1498–1503.
- [17] D. Mellinger and V. Kumar, "Minimum snap trajectory generation and control for quadrotors," in *IEEE International Conference on Robotics and Automation*, May 2011, pp. 2520–2525.
- [18] A. Anta and P. Tabuada, "To sample or not to sample: Self-triggered control for nonlinear systems," *IEEE Transactions on Automatic Control*, vol. 55, no. 9, pp. 2030–2042, 2010.
- [19] N. Bezzo, B. Griffin, P. Cruz, J. Donahue, R. Fierro, and J. Wood, "A cooperative heterogeneous mobile wireless mechatronic system," *IEEE/ASME Transactions on Mechatronics*, vol. 19, no. 1, pp. 20–31, Feb 2014.